Numerical Investigation on the Propulsive Performance of Biplane Counter-flapping Wings

Shuanghou Deng[1*], Tianhang Xiao[2], Bas van Oudheusden[1] and Hester Bijl[1]
[1]Delft University of Technology, Kluyverweg 1, Delft, the Netherlands
[2]Nanjing University of Aeronautics and Astronautics, Yudao Street 29, Nanjing, P.R. China
[*]Email address: s.deng@tudelft.nl

ABSTRACT

A numerical investigation is performed to address the flexing effect on the propulsion performance of flapping wing particularly on the counter-flapping wings of the biplane configuration. A Reynolds number of 10,000 is considered in the present study which corresponds to the flight regime of most existing flapping wing micro air vehicles. The computation involves solving the compressible unsteady Reynolds- averaged Native-Stokes equation using an inhouse developed code. The flapping motion is incorporated by an efficient deforming overset grid technique which allows multiple flexible bodies to be embedded into the flow field. Results show that the biplane wing with counter-flapping configuration has a better propulsive performance in comparison to a single flapping wing. A low-pressure regime between the two wings during the outstroke produces more thrust, while the counter-flapping motion can also generate a surfeit momentum rushing in to the wake. The more flexible wing can produce more thrust while less power is required thus owning a better propulsive performance.

NOMENCLATURE

α_0	flexure amplitude of the airfoil, deg
Cp,a	power coefficient
C_t	thrust coefficient
c	chord length, m
H_0	plunging amplitude
k	reduced frequency, $2\pi f / U_\infty$
U_∞	freestream velocity, m/s
t'	non-dimensional time, tU_∞ / c
η	propulsive efficiency, $C_t / _{Cp,a}$

1. INTRODUCTION

Recently, there is an increasing interest to study micro air vehicle (MAV) configurations in view of their potential in civilian and military applications. The MAV concept can be categorized into three different types, i.e. fixed-wing, rotary- wing and flapping wing MAVs[1]. Flapping-wing MAV (FW-MAV), which is the most intriguing type in the MAV family are considered to have a better aerodynamic performance at the low Reynolds number regime. Like natural flyers, flapping-wing MAV is usually equipped with a single or multiple pairs of flexible wings to generate both thrust and lift at the same time. The flapping locomotion is believed to derive its propulsive performance from some novel unsteady- flow lift enhancement mechanisms[2], such as clap-and-fling (also referred as Weig-Fogh mechanism), delayed stall, wing rotation and wake capture. The propulsive performance of flapping wings has been investigated extensively literature. Lai and Platzer[3], and Jones et al.[4] experimentally studied the thrust production by varying flapping amplitude, oscillation frequency in water-tunnel. Flow-visualizations provided a considerable amount of information about the wake char- acteristics of thrust-producing flapping airfoils. Similar experiment has been conducted by Anderson et al [5], who observed that the phase angle between the plunging and pitch has a significant

role in maximizing the propulsive efficiency. The most common configuration for FWMAVs is to use one pair flapping wings which is biologically mimicked from birds[6][7]. Besides, there are some FWMAVs[8][9] that use a biplane wing layout, which have two pair of wings mounted on both sides of the fuselage that perform a counter-flapping motion. Such configuration is able to generate more thrust and minimizes the rocking amplitude during flight. There are only few studies about the propulsive characteristics of biplane wings perform counter-flapping motion, particularly on flexible wings. This study will focus on the propulsive performance of biplane wing configuration, with emphasis on the propulsive enhancement compared to the single wing configuration. The effect of flexibility on the propulsive of biplane wings will be also briefly addressed.

2. NUMERICAL METHODOLOGY

2.1 Governing equation

For dynamic problems involved with moving or deforming grids, the two most popular methodologies used to tackle such problems, are the Arbitrary Lagrangian Eulerian (ALE) and the dynamic grids. Both approaches are closely related and lead to the same modified form of the governing equations, which accounts for the relative motion of the grid with respect to the fluid. The time-dependent ALE formulation of the Navier-Stokes equations with low Mach preconditioning in integral form reads:

$$\frac{\partial}{\partial t}\int_{\Omega(t)} W dV + \oint_{S(t)} (F(W) - v_g W) dS = \oint_{S(t)} F_v dS \tag{1}$$

here, the conservative variables $W = (\rho,\ \rho u,\ \rho v,\ \rho w,\ \rho e)^T$ while $F\ (W)$ and F_v are the convective and viscous fluxes, respectively; v_g is the contra-variant velocity of the face of the control volume Ω. In order to obtain meaningful solutions for unsteady flow, it is necessary to use a pseudo time approach. Additionally, in the low Mach number regime, schemes for compressible flows have an amount of artificial dissipation which does not scale correctly when the Mach number approaches zero. Thus, the accuracy of such spatial discretization deteriorates at low Mach numbers. This can be remedied, allowing for efficient and accurate solutions at low Mach numbers, by employing a preconditioning method. The advantage of preconditioning is that it enables a solution method, which is applicable at all Mach numbers.

In order to close the N-S equation in the case of turbulent flow, the Spalart-Allmaras (S-A) turbulent model is employed. The pseudotime term τ in the governing equation is discretized with a first order backward difference and the physical time term is discretized in an implicit fashion by means of two step backward difference respectively.

Besides the conservation of mass, momentum and energy, the so-called Geometric Conservation Law (GCL) must be satisfied in order to avoid errors induced by the deformation of control volumes. The integral form GCL reads

$$\frac{\partial}{\partial t}\int_V dV - \oint_S v_g dS = 0 \tag{2}$$

The GCL results from the requirement that the computation of the control volumes or of the grid velocities must be performed in such a way that the resulting numerical scheme preserves the state of a uniform flow, independently of the deformation of the grid. It should be stressed that the GCL is automatically satisfied for such moving grids, where the shapes of the control volumes do not change in time. The GCL is temporally discretized using the same scheme as applied to the governing equations in order to obtain a self-consistent solution method. Note that, for moving boundaries problems, the GCL has to be solved concurrently with the fluid equations.

2.2 Deformable overset grid method

The counter-flapping motion is a relevant mechanism for thrust enhancement and also forms an extreme situation for numerical simulation, where the flexible wings deform strongly during the transition. In the present study, a deformable overset grid strategy[10] is employed to simulate the flapping wing.

2.3 Aerodynamic force and power calculation

The time-average aerodynamic force and power in the present research are defined as

$$\bar{F} = \frac{1}{T}\int_0^T \int_S F(t)dAdt, \bar{P} = \frac{1}{T}\int_0^T \int_S F(t)\dot{x}dAdt \tag{3}$$

where F (t)is the aerodynamic force of a wall element. Furthermore, the thrust coefficient C_T, aerodynamic power coefficient $C_{P,a}$, and propulsive efficiency (the ratio of thrust coefficient to power coefficient) η are given respectively by

$$C_t = \frac{-F_x}{0.5\rho U_\infty^2 c}, \; C_{P,a} = \frac{P}{0.5\rho U_\infty^3 c}, \; \eta = \frac{\bar{C_T}}{\bar{C_{P,a}}} \tag{4}$$

where U_∞ and c are the the incoming frees-stream velocity and the chord length.

2.4 Solver Validation

To assess the accuracy of the method we developed, validation studies were conducted for unsteady flows on moving bodies based on available results in literatures. The unsteady flow fields of a two dimensional rigid NACA0014 airfoil undergoing with a sinusoidally plunging motion as

$$H(t) = H_0 cos(2\pi f t) \tag{5}$$

is simulated under conditions of k = 1, H_0 = 0.4c, *M ach* = 0.1 and Re = 10^4. The computational grid (see in Fig.1) is created with an unstructured mesh with a refinement at the boundary layer region y_+ = 1. The mesh was moved entirely during the computation to follow the specific plunging equation.

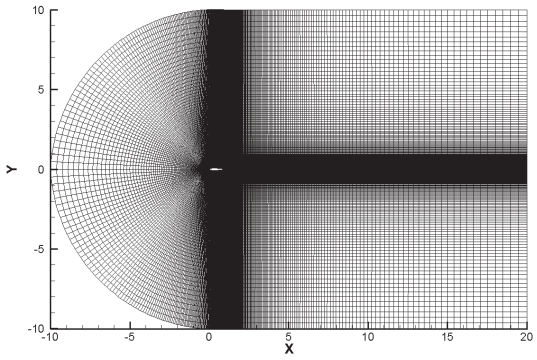

Fig. 1: NACA0014 computational mesh.

The computed results in terms Mach contour distribution and temporal drag coefficients are compared with those obtained by Tuncer and Kaya[11] using overset grid in Fig.2and Fig.3. As can be seen that, the drag coefficients variations over time and the Mach contour are in reasonably good agreement with the reference results.

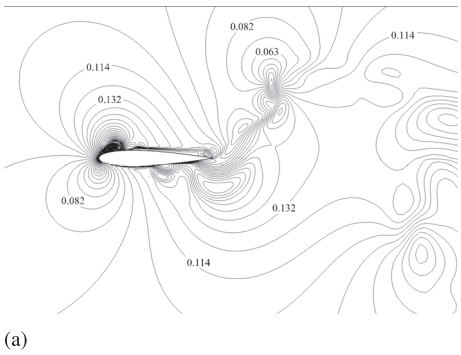

(a)

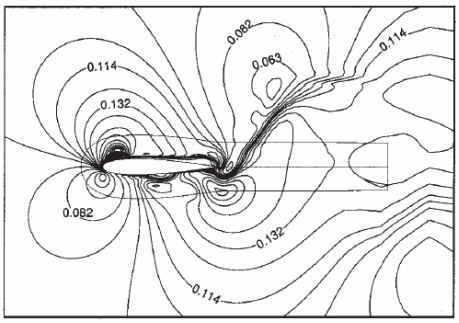

(b)

Fig. 2: Mach contour comparison at $H(t) = 0.0$, downstroke: (a)present results; (b)Tuncer and Kaya [11].

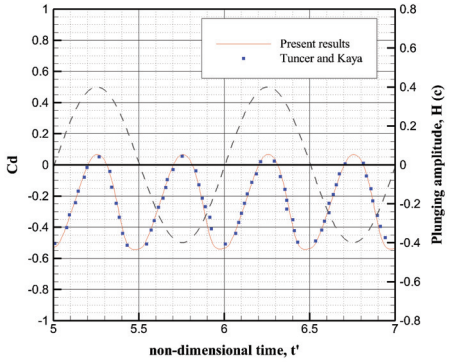

Fig. 3: Drag coefficient comparison for two flapping cycles.

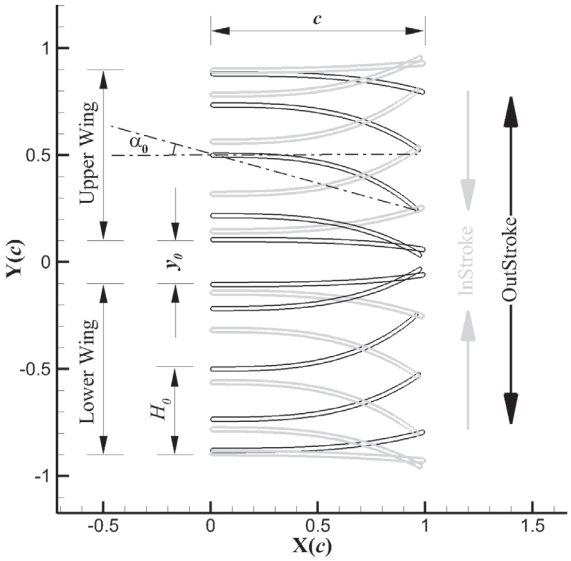

Fig. 4: Illustration of counter-flapping wings.

2.5 Computational setting

Two thin flat plates are used in the present study to represent the flexible wings, see in Fig.4. The upper and lowers wings perform a mirroring flapping pattern with respect to the bisector line ($Y = 0$). The motion pattern can be found in Eqn(6) and (7) , where the $\alpha(x, t)$ stands for the instantaneous local slope angle and which reflects the chordwise deformation, while H_0 denotes the plunging amplitude, which stays at a constant of 0.4 chord length in this paper. Note that in order to avoid the wing crossing at their nearest location, the minimal clearance between the wings y_0 was set to 0.2c.

$$H(t) = H_0 sin(2\pi ft) \tag{6}$$

$$\alpha(x,t) = \alpha_0 (\frac{x}{L})^2 sin(2\pi ft - 90^\circ) \tag{7}$$

Two computational settings are used in the present paper, i.e. a single wing flap motion (hereafter referred to as **SW**); and a counter-flapping biplane wing configuration(hereafter referred to as **BW**). The object of the present study is to 1) address the propulsive characteristics i.e. thrust, power and efficiency of the **BW** configuration, when compared with the **SW** layout; 2) examine the effect of flexibility on the propulsion performance of the **BW** configuration. The parameters set-up for the flapping wings in the present study are shown in Table1. Note that the Strouhal number St and the reduced frequency k are fixed at 1.3 and 2, respectively to isolate the effect of flexibility. The flapping amplitude α_0 ranges from 5° to 15° with an increment of 5° so as to vary the flexibility level.

Tab. 1: Parameter setup for the flapping wings.

Parameter	Value
Re	10,000
k	2
St	1.3
α_0	$5 \sim 15°$
H_0	$0.4c$

The computation background mesh size is $80c \times 60c$ with a fine Cartesian grid filled in the middle region where the flapping wings are located, while the far-field is filled with large scale triangular grids to decrease the cell number, see Fig.5(a). Since we are running the computation at $Re = 1 \times 10^4$, the wall boundary is refined with $y_+ = 1$ boundary layers as shown in Fig.5(b). The total mesh cell amount is 200,000 and computations are run on a 8 cores Windows7 PC.

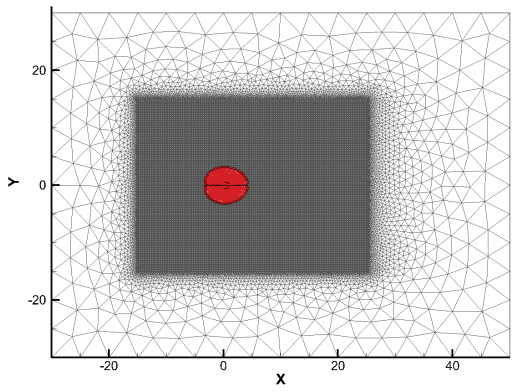

(a)

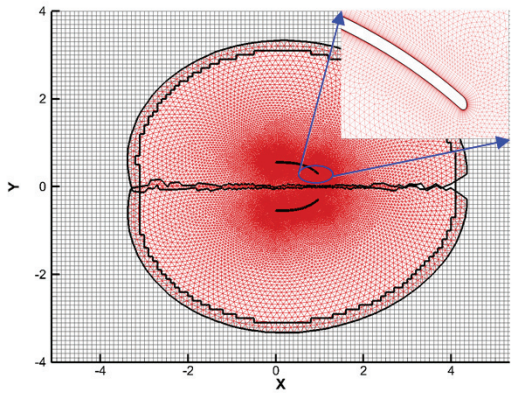

(b)

Fig. 5: (a) Overset grid system at certain time moment; (b) Zoom in view and the boundary layer refinement illustration.

3. RESULTS AND DISCUSSION

Instantaneous vorticity contours for both **SW** and **BW** configurations are plotted in Fig.6 to support the discussion of the unsteady flow features. The development of the leadingedge vortex (LEV) and the trailing-edge vortex (TEV) around the wings are clearly observed. As expected, the predicted flow-field is symmetrical with respect to the bisector line for **BW** configuration. The flow structures of the **SW** is quite similar as for the **BW** on the outer portion. Notable different structures are observed at the inner portion, where the region is significantly influenced by the wing-to-wing interaction. A strong TEV is generated for the **BW** configuration (Fig.6(b)) which is not presented in the **SW** case. Such TEV may result from the low pressure region between the wings hence ingesting the flow around the trailing edge. At the end of the outstroke, the vortex shed from the aft (Fig.6) can be regarded as an indicative of drag production. Due to the relatively higher velocity caused by the **BW** moving instroke, the vortices attached on the inner part (see Fig.6(f)) will be gradually 'squeezed' towards the trailing edge which will produce thrust. Moreover, the counter-flapping motion will enlarge the core size of the LEV in both instroke and outstroke.

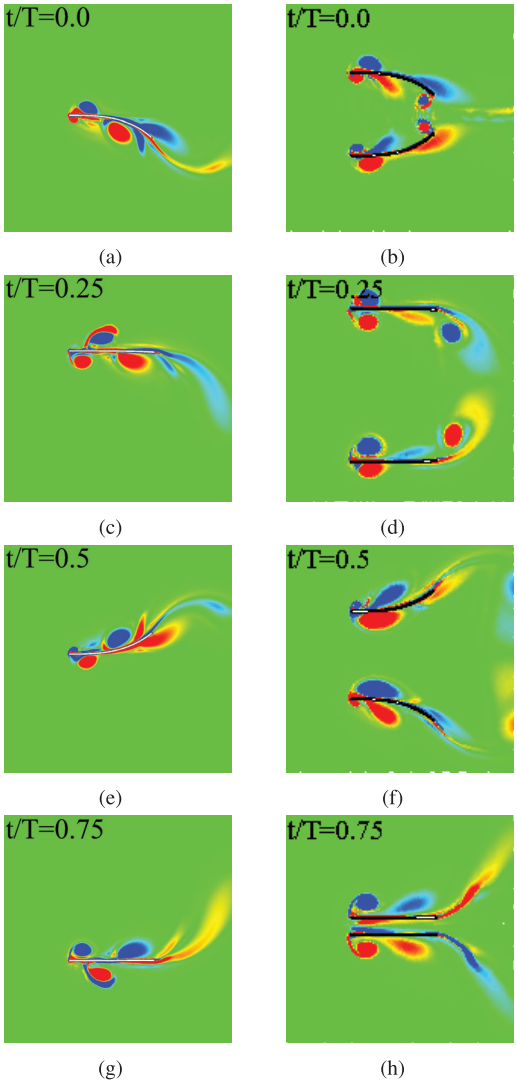

Fig. 6: Vorticity contour for SW and BW configuration during one flapping cycle.

Fig.7displays the far-field wake structure for both the **SW** and **BW** configurations by vorticity contour. The reversed von Karman vortex street was observed: one row in the SW and two rows in the **BW** configuration, which is associated to the generation of thrust.

The thrust, power and their ratio (η) of both SW and BW configurations are presented in Table.2 for comparison. It can be seen that the **BW** wing has a significant increase in the thrust generation, say more than twice of the **SW** configuration. Moreover, the propulsive efficiency is also higher. The results illustrate the wing to wing interaction of the counter-flapping event is beneficial on the propulsive performance.

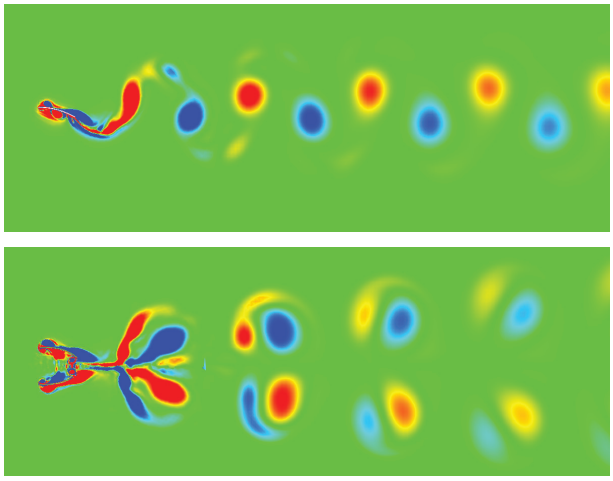

Fig. 7: Vorticity contour in the wake, Top:**SW**; Bottom:**BW**.

Tab. 2: Propulsive performance of SW and BW configurations.

Parameter	**SW**	**BW**
C_t	0.204	0.662
$C_{p,a}$	0.817	2.180
η	0.25	0.30

To further understand the propulsive enhancement due to the counter-flapping, the pressure distribution during outstroke and the velocity during instroke in the coming freestream direction are plotted in Fig.8. As the wings start separating from each other, a low pressure field is formed between the wings, especially at the leading and trailing edges, see in Fig.8(b). Such low pressure region can create a high suction force toward the incoming free-stream direction, thus contributing to thrust. The low pressure inside the curvature of the **SW** is found also, however, quite smaller compared to the **BW** configuration. Fig.8(c) and (d) depict the x-velocity contour during instroke. The counter-flapping event from the **BW** creates a relative stronger flow rush into the wake, which can be regarded as a surfeit momentum augment when compared with the **SW** case.

Fig.9 plots the period-averaged velocity profile in the wake of both **SW** and **BW** configurations. The data was obtained on a slice vertically oriented at one chord length after the trailing edge. The **BW** wake velocity shows two peaks due to the presence of the two wings, with roughly more than twice of the **SW** case in term of magnitude.

Fig.10 shows the variation of the period-averaged thrust, power and propulsive efficiency of the **BW** configuration with respect to the flexibility (indicated by α_0). As shown, the thrust and propulsive increase with increasing flexibility level within the tested range, i.e. $\alpha_0 = 5 \times 15^o$, while the aerodynamic power input illustrates a reversal tendency, more rigid wings requires more power during flight.

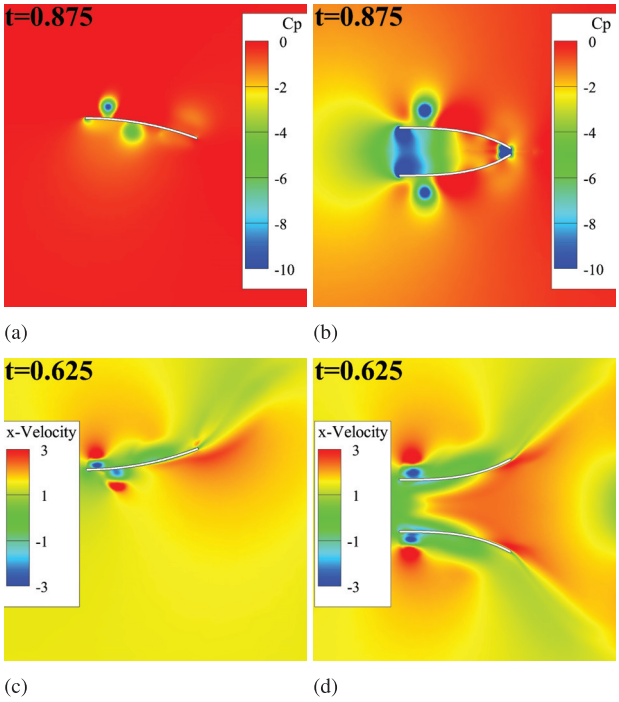

Fig. 8: Pressure and velocity contour comparison: (a) SW Pressure; (b) BW Pressure; (c) SW x-Velocity; (d) BW x-Velocity.

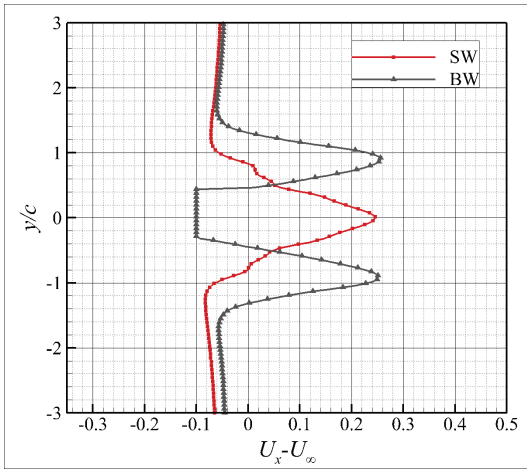

Fig. 9: Period-averaged mean velocity magnitude distribution for SW and BW configurations.

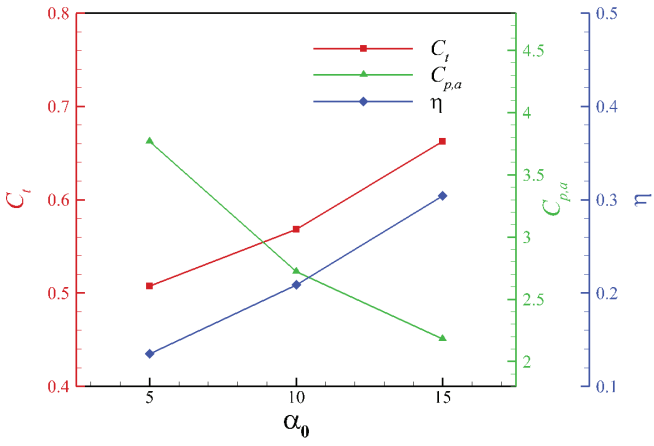

Fig. 10: Effect of flexibility on the thrust, power and propulsive efficiency of BW configuration.

4. CONCLUSION

A numerical investigation was conducted on flexible counter-flapping wings which is a suitable configuration for flapping wing MAVs. The goals are to 1)address the propulsive characteristics between the single wing and biplane wing configurations; 2) examine the effect of flexibility on the propulsive characteristics of biplane flexible wings. The simulation was achieved by solving a low Mach preconditioned URANS solver and coupled with an advanced deformable overset grid technique. All the computations were performed under the condition: $Re = 10,000$, $k = 2$, $H_0 = 0.4c$, $St = 1.3$, the pitching angle varied from $5 \sim 15$ *degs* in this study to identify the flexibility level. Results indicate that the counter-flapping motion can significant enhance the thrust production, which the reason is concluded in terms of flow structure. More flexible wings can generate more thrust while

require less power Thus, the efficiency (i.e. thrust to power ratio) is increased with the increasing flexibility. The thrust, power and efficiency shows a monotonic trend in the defined flexibility range considered in our study. This motivates a further coherent study to parametrically investigate the propulsive characteristics of flexible flapping wings.

ACKNOWLEDGEMENTS

This work has been supported by the Netherlands Technology Foundation (STW, project number 11023) and the National Science Foundation of China (No.11002072). The support from China Scholarship Council (CSC, No. 2011683005, No. 201303070173) is also appreciated.

REFERENCES

[1] Mueller, J.T.(ed.), *Fixed and flapping wing aerodynamics for Micro Air Vehicles*, Progress in Aeronautics and Astronautics, Vol.195, AIAA, Reston, VA, 2001.

[2] Sane, S.P., *The aerodynamics of insect flight*,Journal of Experimental Biology, Vol. 206, 2003, pp.4191-4208.

[3] Lai, J.C.S, Platzer, M.F., *The characteristics of plunging airfoil at aero free-stream velocity*, AIAA Journal, Vol. 39, No. 3, 2001, pp. 531-534.

[4] Jones, K.D., Dohring, C.M., and Platzer, M.F.,*An experimental and computational investigation of the Knoller- Betz effect*, AIAA Journal, Vol. 36, No. 7, 1998, pp. 1240-1246.

[5] Anderson, J.M., Streitlien, K., Barrett, D.S., and Triantafyllou, M.S.,*Oscillating foils of high propulsive efficiency*, Journal of Fluid Mechanics, Vol. 360, 1998, pp. 41-72.

[6] Pornsin-Sirirak, T N., Tai, Y.C., Ho, C.M., and Keenon, M., *Microbat A palm-sized electrically powered ornithopter*, NASA/JPL Workshop on Biomorphic Robotics, August 14-17, 2001, Pasadena, CA.

[7] Gafford, J.B., Kesner, S.B., Wood, R.J., and Walsh, C.J., *Microsurgical Devices by Pop-up Book MEMS*, Proceedings of the ASME 2013 International Design Engineering Technical Conferences & Computers and Information in Engineering Conference, August 4-7, 2013, Portland, Oregon, USA.

[8] De Croon, G.C.H.E, Groen, M.A., De Wagter, C., Remes, B., Ruijsink, R., and van Oudheusden, B.W., *Design, Aerodynamics, and Autonomy of the Delfly. Bioinspiration and Biomimetics*, Vol. 7, No.2 , 2012, pp. 1-16.

[9] Ren, H., Wu, Y., and Huang, P.G., *Visualization and Characterization of Near-wake Flow Fields of a Flapping-wing Micro Air Vehicle Using PIV*, Journal of Visualization, Vol. 16, 2013, pp. 75-83.

[10] Deng, S., Xiao, T., van Oudheusden, B.W., Bijl, H., and Remes, B., *Numerical simulation of DelFly flapping wing MAV by means of a deforming overset grid method*, 22nd AIAA Computational Fluid Dynamics Conference, 22-26 June, Dallas, US.

[11] Tuncer, I.H., Kaya, M.,*Thrust Generation Caused by Flapping Airfoils in a Biplane Configuration*, Journal of Aircraft, Vol.40, No. 3, pp. 509-515, 2003.